# Abstract

Modern telecommunications networks maintain synchronization and distribute accurate timing information using approaches with strict requirements on clock quality and jitter and wander at interfaces. In the future, packet networks may be used for timing distribution and synchronization e.g. using IEEE 1588v2 specifying the Precision Time Protocol (PTP). Without amelioration, there may be effects on data buffers within telecommunications networks which have been designed with particular assumptions of clock quality. Applications such as digital audio and video also have synchronization requirements and limits on jitter and wander tolerance. Attention is needed on the impact of clock quality due to clock synchronization on the synchronization and jitter and wander limits for data services over networks. A well-understood approach to the transfer of timing for a data service over a packet network is the Synchronous Residual Time Stamp (SRTS) method. We previously presented a novel approach to modelling and visualising jitter spectra in SRTS timing transfer due to jitter in the reference clocks. In this paper, we present experimental results, which validate the appropriateness of our approximations. Experimental results also show the existence of some spectral components not predicted from the modelling. In the paper we discuss the origins of these spectral components.



Keywords: synchronization, jitter, timing, frequency modulation, networks, timing jitter precision time protocol, network timing, wander, SRTS

# Experimental evaluation of the jitter generated in timing transfer.

Jacqueline Walker, *Member, IEEE* and Antonio Cantoni, *Fellow, IEEE*

## I Introduction

Modern telecommunications networks currently maintain synchronization and distribute accurate timing information using the traditional approach of the Synchronous Optical Network (SONET)/Synchronous Digital Hierarchy (SDH) [1], [2]. These networks have strict requirements on the quality of clocks used at various levels of the hierarchy [3] and on the control of jitter and wander at interfaces [4]. However, in the future, it is envisaged that timing distribution and synchronization may occur over a packet network such as IEEE 1588v2 specifying the Precision Time Protocol (PTP) [5]. IEEE 1588 provides for a variety of mechanisms to allow a slave clock to synchronize to a master clock via the exchange of time stamp information. In [5], it is shown that variable packet delay may have a substantial influence on the quality of the slave clock by introducing extremely low-frequency wander which may pass through the local servo control loop and affect the resulting local slave clock output. The implication is that, without amelioration, there may be an effect on data buffers within telecommunications networks which have been designed with particular assumptions of clock quality [5].

From the point of view of applications, such as digital audio and video services, transferred over networks using IEEE 1588, there are also synchronization requirements as well as limits to the amount of jitter and wander which can be tolerated [6]. For example, in Audio/Video Bridging (AVB) networks, uncompressed digital video requires peak-to-peak jitter $< 1\,\text{ns}$ and wander of $\leq 1\,\mu\text{s}$ over a period of $\leq 10\,\text{s}$ [6]. Currently, the high quality telecommunications networks timing references are also often relied upon to provide syntonization and even synchronization to wireless base stations and the jitter and short-term wander requirements

are, in most cases, similar to those for AVB applications [6]. Thus, attention needs to be paid to the impact of clock quality due to clock synchronization techniques on the synchronization and jitter and wander limits for data services transferred over networks.

An example of a well-studied approach to the transfer of a data service over a packet network is the transfer of timing information for constant bit rate (CBR) transmission over ATM Adaptation Layer 1 (AAL1) by the Synchronous Residual Time Stamp (SRTS) method [7]. The transfer of the necessary timing information for the data service (constant bit rate audio and/or video) from source to destination involves encoding the timing information at the source using a local reference clock and reconstructing the source clock at the destination using the encoded information and a reference clock available at the destination. It has been shown that the generation of the time stamp requires the synchronization of one clock, known as the service clock, into the domain of the local reference clock and thus is similar to rate adaptation by bit stuffing [8], [9] and pointer adjustment [10] and that the jitter generated is similar to waiting-time jitter [7], [8]. Waiting-time jitter is deterministic and can accumulate significantly from repeater to repeater [11], whereas jitter accumulation in synchronous networks is prevented by limiting the number of allowed pointer adjustments [10].

In previous analyses, the focus was on the timing transfer process itself and the effect of the resulting waiting-time jitter on the recovered service clock [8], [9] and it has usually been assumed that the reference clocks used in the timing transfer process are ideal. Within the context of synchronization of networks using newer approaches such as IEEE 1588, packet delay jitter may affect the transmission of time stamps both for the synchronization of the slave clock (i.e., the destination reference clock in the SRTS model described above) [5] as well as the timing transfer for the service clock itself [6].

In [12], consideration was given to the effect of jitter on the service clock itself and the

predictions for the spectral characteristics of the jitter were validated by experiment. In [13], the effect of jitter on the reference clocks, both at source and destination was considered. The analysis involved certain approximations and assumptions, which were different for the two cases (i.e., source and destination reference clocks).

In this paper, we present experimental results which validate the appropriateness of the approximations used in the analysis in [13] and confirm the jitter spectra predicted in that paper. We focus on jitter spectra as jitter and wander performance requirements are frequently specified in the frequency domain [4] and jitter spectra can readily be converted to other measurements [14] and are often used to specify the performance of end-to-end timing transfer in communications systems [15], [16]. The experimental results also show the existence of some spectral components that were not predicted in the modelling carried out in [13]. In the paper we discuss the origins of these spectral components. The value of experimental work in identifying omissions in theoretical models and the strength of assumptions in modelling is clear.

The paper is structured as follows, in Section II, we present a brief overview of the analytical results from [13], highlighting the assumptions made in the analysis; in Section III, the experiments are described and results are presented. Finally, a concluding discussion is presented in Section IV.

## II. Theoretical Background

In this section we briefly review the theoretical findings on the jitter spectra in synchronization for the cases of both ideal and non-ideal reference clocks. The rate adaptation process is illustrated in the timing diagram in Fig. 2 where the divided-down service clock period $T$ is synchronized to the reference clock of period $T_{nx}$. As the exact number of reference clock cycles in $T$ is usually not an integer, the result is a quantized representation

of the service clock with inter-pulse intervals $S_n T_{nx}$, where $S_n$ takes on one of two possible values: $\lfloor M \rfloor$ or $\lfloor M \rfloor + 1$, such that its long term average period is $M$ [9]. The resulting jitter on the quantized service clock, $d_n T_{nx}$ (denominated in seconds), is also the jitter present on the recovered timing signal at the destination when the reference clocks are assumed ideal and $d_n$ is given by:

$$d_n = (d_0 - nM) - \lfloor d_0 - nM \rfloor \tag{1}$$

The resulting quantization jitter $d_n T_{nx}$ has a spectrum given by [9]:

$$J(f) = F \sum_{k=-\infty}^{\infty} \alpha_k \sum_{n=-\infty}^{\infty} \delta(\bar{f} - k\rho - n) \tag{2}$$

where $\bar{f} = f/F$ is the normalised frequency, $F = 1/T$, $\alpha_k = \begin{cases} T_{nx}/2, k = 0 \\ T_{nx} e^{-j2\pi k d_0} / j2\pi k, k \neq 0 \end{cases}$ and

$$\rho = \frac{T}{T_{nx}} - \left\lfloor \frac{T}{T_{nx}} \right\rfloor. \tag{3}$$

In Fig. 1, the waiting-time jitter spectrum is shown for ideal clocks. The top plot shows the spectrum calculated from equation (1) and the bottom plot shows the spectrum plotted from experimental data (using the same approach as described in Section III) with unjittered clocks. The variance of the waiting-time jitter is $T_{nx}^2/12$ and, due to its sawtooth characteristic, its peak-to-peak value and MTIE (Maximum Time Interval Error) are constrained to be no more than $T_{nx}$ seconds. The characteristic spectrum of this kind of timing jitter, known as waiting-time jitter [7]-[9] is set by the value of $\rho$ and typically consists of many spectral lines with aliasing to low frequencies due to the undersampling at the rate of the divided-down service clock.

### A. Jittered Destination Reference Clock

A service clock which has been encoded and transmitted will be regenerated at the

destination. Regardless of the physical details of the implementation of the regeneration, it will necessarily involve the use of a destination reference clock which will reproduce the encoded service clock period as a sequence, $S_n$, of reference clock cycles. As shown in the timing diagram in Fig. 2, when the reference clock at the destination is jittered, the resulting jitter on the service clock at the destination will be $w_n T_{nx} = d_n T_{nx} + \phi(t_n) T_{nx}$, where $\phi(t_n) T_{nx}$ is a sample of the jitter on the reference clock at $t_n = nT + d_n T_{nx}$. Thus the jitter on the reference clock is effectively sampled non-uniformly at time instants determined by the value of the jitter on the reconstructed timing signal. The non-uniformly sampled jitter function can be written as $\phi_s(t) = \sum_{n=-\infty}^{\infty} \phi(t_n)\delta(t - t_n) = \phi(t) \sum_{n=-\infty}^{\infty} \delta(t - t_n)$ and in general its spectrum is given by [17]:

$$\phi_s(f) = \Phi(f) \otimes F\left\{ \sum_{n=-\infty}^{\infty} \delta(t - t_n) \right\} \tag{4}$$

where $\Phi(f)$ is the spectrum of the uniformly sampled reference clock jitter, $\otimes$ represents convolution and $F\{\ \}$ represents the Fourier Transform. In [13], we showed that the spectrum of the non-uniformly sampled jitter, $\phi(t_n)$, can be determined approximately by using the nonlinear time transformation originally developed by Papoulis [18] to give:

$$F\{\phi(t_n)\} = \left(\Phi(\bar{f}) + \Theta(\bar{f}) \otimes j2\pi\bar{f}\Phi(\bar{f})\right) \otimes F \sum_{n=-\infty}^{\infty} \delta(\bar{f} - n) \tag{5}$$

where $\Theta(f)$ is the spectrum of the lowpass filtered waiting-time jitter in (2). Based on (5) we predict that the spectrum of the non-uniformly sampled reference clock jitter will be the spectrum of the reference clock jitter convolved with a lowpass filtered waiting-time jitter spectrum. This spectrum is dominated by the spectral peaks due directly to the sinusoidal jitter on the destination reference clock, i.e. the feed-through sinusoidal jitter. The spectral lines from the waiting-time jitter are lowpass filtered and convolved with the feed-through

jitter peaks. Thus, these spectral lines appear relative to the feed-through jitter peaks.

For the analyses in [13] and for the experiments, sinusoidal jitter was used as the jitter applied to the destination reference clock because it represents a conservative estimate of jitter effects as it spends more time closer to its peak values [19] and because it allows for closed-form calculation of the jitter spectrum. Due to the presence of feed-through jitter, the maximum peak-to-peak jitter expected is given by $T_{nx} + 2A_j$ and the MTIE(S) is $T_{nx} + 2A_j$ for $S \geq 1/2f_j$. The expected variance of the jitter, including the feed-through jitter term, is $\frac{A_j^2}{2} + \frac{\left(T_{nx} A_j f_j \pi\right)^2}{12}$.

### B. Jittered Source Reference Clock

The effect of jitter on the source reference clock on the synchronization process and the resulting jitter on the quantized service clock is shown in Fig. 3. In [13], to facilitate the analysis when the reference clock at the source is jittered, the equivalence of the synchronization process to a first-order sigma-delta modulator was used [9], [20]. It was shown that the jitter spectrum is of the same form as that for the jitter generated when there is timing jitter on the service clock itself. In the specific case of jitter on the source reference clock, the spectrum can be approximated as:

$$J(f) = F \sum_{n=-\infty}^{\infty} \sum_{k=-\infty}^{\infty} \alpha_k \sum_{m=-\infty}^{\infty} J_m(2\pi k\gamma) \delta\left(\bar{f} - k\rho - n - m\frac{f_j}{F}\right) \qquad (6)$$

where $J_m(x)$ are Bessel functions of the first kind and $\gamma = f_{nx} 2\pi f_j A_j / \left(2F \sin\left(\pi f_j T\right)\right)$ where the jitter is low-amplitude sinusoidal timing jitter that can be approximately represented as phase jitter [12], [21]. This spectrum thus contains additional aliasing of the spectral lines of the waiting-time jitter spectrum at multiples of the normalized jitter frequency and with amplitudes determined by Bessel functions of the first kind leading to an appearance similar

to that of a frequency tone modulation spectrum. It is straightforward to show that the variance of the modified waiting-time jitter in this case is still given by $T_{nx}^2/12$. However, due to the presence of feed-through sinusoidal jitter, the maximum peak-to-peak jitter expected is now given by $T_{nx} + 2A_j$ and the MTIE(S) is $T_{nx} + 2A_j$ for $S \geq 1/2f_j$.

## III. Reference Clock Jitter Experiments

To test the predictions for the effect of reference clock jitter on the jitter spectrum of the regenerated service clock, a service clock timing transfer system (the Synchronous Residual Time Stamp (SRTS) from the ATM Adaptation Layer 1 [7], [22]) was implemented on an Altera EP20K400EFC672-2X FPGA. The general experimental configuration is shown in Fig. 4; note that both the SRTS generation and re-generation modules were implemented on the same chip and the SRTS is transferred directly between them. As the intention is to study the effect of jitter in the reference clocks on the SRTS output jitter, it is useful to ensure that there are no channel effects on the SRTS output jitter. The clock rates used are from the specifications for AAL1 in [22]. The 77.76 MHz reference clocks at source and destination were provided by an HP ESGD-4000A Signal Generator and an HP8644B High Performance Signal Generator; specific experimental configurations are summarised in the tables below. The reference clocks at source and destination were locked to each other as they would be in a telecommunications network where they would be slaved to a higher level master clock. A high rate service clock signal (44.736 MHz) was provided by a second HP ESGD-4000A and was divided down by 3008 in the SRTS generation procedure [7] resulting in a divided-down service clock of frequency 14872.34 Hz.

Experiments were conducted for different values of $\rho$ (0.05, 0.007 and 0.321879) in order to verify theoretical predictions made and previously confirmed using only Matlab simulations [13]. The HP5372A Frequency and Time Interval Analyser was used to make time interval

measurements from Channel A to Channel B, resulting in data which is an indexed list of the time interval in seconds from the edge of the divided-down service clock to the edge of the regenerated destination divided-down source clock. Thus, these measurements include the jitter between the divided-down service clock at the source and the regenerated service clock at the destination as illustrated in Fig. 2.

Matlab was used to obtain plots of the spectrum of the jitter from the experimental data. The time interval measurements were imported into Matlab, 2048 points of the jitter data were windowed with a 2048-point Hamming window and a 2048-point FFT taken [23]. The predicted spectra were plotted from the applicable equations in Section II using the same approach as used by the authors in [13]. In the case of jitter on the destination reference clock an additional plot of the jitter spectrum predicted by simulation was generated as follows. Sinusoidal time jitter of amplitude and frequency corresponding to that used in the experiment was simulated and sampled non-uniformly using the waiting-time jitter samples generated using the value of $\rho$ set in the experiment. The resulting jitter samples (feed-through waiting-time jitter plus the non-uniformly sampled sinusoidal jitter) are windowed by a 2048-point Hamming window and a 2048-point FFT taken.

### A. Jitter on the Source Reference Clock

The experimental configuration for measuring the effect of jitter on the source reference clock is summarised in Table 1.

| Clock | Equipment | Nominal Frequency (MHz) | Applied Modulation |
|---|---|---|---|
| Service clock | HP ESGD-4000A | 44.736 | None |
| Source reference clock | HP ESGD-4000A | 77.76 | Sinusoidal FM<br>$f_j = 4000$ Hz, $\beta = 0.566$ , $\Delta f = 2262$ Hz<br>$A_j = 0.09$ UI, 1 UI = 12.8 ns |
| Destination reference clock | HP 8644B | 77.76 | None |

**Table 1: Experimental set-up for measurement of jitter on the source reference clock.**

The theoretical predictions and simulations presented in [13] were for a sinusoidal timing jitter frequency of 20 Hz at an amplitude of 0.09 UI, i.e. corresponding to a low-level low frequency jitter. The scaling up of the jitter frequency was necessary because at 20 Hz, the required peak frequency deviation ($\Delta f$) was 11.31 Hz (modulation index $\beta = 0.5655$), which was too small for the HP ESGD-4000A to produce. It is straightforward to confirm that these jitter settings still meet the conditions under which frequency modulation can be used to approximate timing jitter. These conditions are [12]:

$$f_j A_j << \frac{1}{2\pi}$$
$$f_j T_{nx} << \frac{1}{2\pi} \qquad (7)$$

Here $f_j A_j \approx 4.6\times10^{-6}$ and $f_j T_{nx} \approx 5.1\times10^{-5}$.

*1) Results of Jittered Source Reference Clock Experiments*

During the experiments, measurements were taken of the average frequency and period of the service clock and the regenerated service clock using the HP5372A. These measurements agreed with the settings of the instruments, as shown in Table 2 below, to within $\pm 0.10$ Hz. The discrepancy between the measured average frequency of the divided-down service clock at the source and the regenerated service clock at the destination is $\leq \pm 0.25$ Hz.

| (Higher-rate) Service clock (as set at source) (MHz) | (Divided-down) Service clock (calculated) (Hz) | (Divided-down) Service clock (as measured) (Hz) | $\rho$ (as set) | $\rho$ (calculated for source) | (Regenerated divided-down) Service clock (as measured) (Hz) |
|---|---|---|---|---|---|
| 44.74020020 | 14873.74 | 14873.65 | 0.007 | 0.0375 | 14873.60 |
| 44.73983225 | 14873.61 | 14873.60 | 0.05 | 0.055 | 14873.65 |
| 44.73750573 | 14872.84 | 14872.76 | 0.321879 | 0.350353 | 14873.69 |

**Table 2: Summary of Source Reference Clock jitter experiments.**

The value of $\rho$ determines the appearance of the jitter spectrum. As $\rho = \langle f_{nx}/F \rangle$, even quite small changes in the frequency of the service clock used in this equation can produce large changes in the value of $\rho$. To determine whether the average frequencies as measured by the HP5372A (see Table 2) should be used, the spectra of the experimental data for a given $\rho$ (as determined by the *frequency settings* of the experiment) were compared with predicted spectra plotted for that $\rho$ value and with predicted spectra plotted with $\rho$ values calculated from the *average measured* frequencies. As shown in Fig. 5, the experimental spectra correspond to the value of $\rho$ based on the frequency settings on the equipment, rather than with the value of $\rho$ calculated from the average frequency measurements.

The predicted value of the peak-to-peak jitter and MTIE was $T_{nx} + 2A_j$, the value found from the experimental data was $1.56 \times 10^{-8}$ sec. The predicted variance of the jitter was $T_{nx}^2/12$ and from the experimental data, the mean of the variances of the jitter over the three different values of $\rho$ considered was found to be $1.45 \times 10^{-17} s^2$

*2) Differences between predicted and experimental spectra*

In Fig. 6, predicted and experimental spectra are plotted for two further values of $\rho$. The main difference between prediction and experiment observed in both cases was the presence of spectral peaks at normalised frequencies of 0.2698 and 0.731 in the experimentally

produced spectrum. The normalised frequencies at which these peaks occur correspond to $\pm f_j$ and appear to be the spectral peaks of the sinusoidal jitter affecting the source reference clock, i.e. they are a feed-through jitter component. The occurrence of these peaks was not originally predicted due to the analysis method used (as described in Section II.B.) and consequently they do not appear in the predicted spectra plots of Fig. 6. Unlike the situation when there is jitter on the service clock [12], it is not immediately apparent even from the timing diagram in Fig. 3, that the jitter on the quantized service clock at the source includes a feed-through component (denoted $e_n T_{nx}$) of the sinusoidal jitter on the source reference clock (where $e_n = A_j \sin(2\pi f_j nT)$). However, as the situation of jitter on the source reference clock can be transformed into a representation where the source reference clock is ideal and the jitter is applied to the service clock, it is apparent that there should be a feed-through jitter term as was found in the experiments and this will appear in the spectrum with amplitude of $F(A_j/2)$, independent of the value of $\rho$. For the parameters used in the experiment, the amplitude of the feed-through jitter peaks is predicted to be approximately $8.6\times10^{-6}$ which is the size of the observed spectral peaks in all cases, i.e. the amplitude of these peaks is independent of the value of $\rho$.

### B. Jitter on the Destination Reference Clock

The experimental configuration for measuring the effect of jitter on the destination reference clock is summarised in Table 3. Although this is clearly no longer narrowband frequency modulation with respect to the reference clock, the jitter settings still meet the conditions under which frequency modulation can be used to produce timing jitter. From (7), we have $f_j A_j \approx 9.3\times10^{-4}$ and $f_j T_{nx} \approx 5.1\times10^{-5}$.

| Clock | Equipment | Nominal Frequency (MHz) | Applied Modulation |
|---|---|---|---|
| Service clock | HP ESGD-4000A | 44.736 | None |
| Source reference clock | HP 8644B | 77.76 | None |
| Destination reference clock | HP ESGD-4000A | 77.76 | Sinusoidal FM $f_j = 4000$ Hz, $\beta = 113$, $\Delta f = 452.4$ kHz $A_j = 18$ UI, 1 UI = 12.8 ns |

**Table 3: Experimental set-up for measurement of jitter on the destination reference clock.**

The parameters used for the predictions and simulations in [13] were for a jitter frequency of 20 Hz at an amplitude of 18 UI, i.e. corresponding to a high-level wander signal. A larger amplitude jitter was required for the jittered destination reference clock experiments in order to be able to visualise the extremely small aliased waiting-time jitter peaks in the non-uniformly sampled input jitter spectrum. The jitter frequency was increased to 4000 Hz to make the main jitter peak more clearly visible. When a jitter frequency of $f_j = 20$ Hz is used, since $f_j / F = 0.00135$, the main feature of the spectrum was too close to the edges of the plot and as a result it was difficult to visualise much of the structure of the plot.

*1) Results of Jittered Destination Reference Clock Experiments*

In Fig. 7, predicted, simulation and experimental spectra are plotted for $\rho = 0.321879$. The main features in the spectra are the spectral peaks due to the feed-through sinusoidal jitter applied to the reference clock at the destination. The feed-through waiting-time jitter ($d_n T_{nx}$ in Fig. 2) is very small in comparison and, at the scale used (vertical axis maximum = 0.002), can barely be seen. In Fig. 8, 'close-ups' at a different scale (vertical axis maximum = $2 \times 10^{-5}$) are shown which clearly indicate that the predicted spectrum agrees with the experimental result. Note that the main additional feature of the plot visible at this scale is the

feed-through waiting-time jitter; $d_n T_{nx}$, the aliased waiting-time jitter peaks due to the non-uniform sampling of the jitter on the reference clock ($\phi(t_n)T_{nx}$) in Fig. 2 are the much smaller peaks visible in the predicted and simulated spectra. In the spectrum plotted from the real experimental data, the peaks are present but are within the noise floor of the FFT.

The predicted value of the peak-to-peak jitter and MTIE was $T_{nx} + 2A_j$, the value found from the experimental data was $4.8 \times 10^{-7}$ sec. The predicted variance of the jitter was $\frac{A_j^2}{2} + \frac{\left(T_{nx} A_j f_j \pi\right)^2}{12}$ and from the experimental data, the mean of variance of the jitter over the three different values of $\rho$ considered is $2.7 \times 10^{-14} s^2$.

*B. Differences between predicted and experimental spectra*

In Fig. 9, predicted and experimental spectra are plotted for $\rho = 0.05$ and $\rho = 0.007$. The vertical axis scale is adjusted to focus on the detail of the feed-through waiting-time jitter peaks. It may be noted that there are spectral peaks present in both experimental spectra which are not present in either the predicted or the simulation spectra (also shown). Regardless of the value of $\rho$, the peaks are present at the same normalised frequency points: $\bar{f} = 0.4625$ and $\bar{f} = 0.5375$. These points correspond to $F \pm 2f_j$ and must be due to the frequency modulation used to produce timing jitter in the experiment. The simulation data does not produce these lines in its spectrum because it is a time-domain simulation in which waiting-time jitter samples are generated and used to sample sinusoidal 'jitter' in an analogous manner to how it occurs in the SRTS regeneration process.

As can be seen from Fig. 2, due to the jitter on the destination reference clock, the reconstructed destination service clock is also jittered and this jitter consists of the fed-through original waiting-time jitter and the applied input sinusoidal jitter affecting the

destination reference clock. The peak amplitude of the sinusoidal jitter in time is $18 \times 12.86 \times 10^{-9} = 0.23\mu s$, and the peak amplitude of the feed-through waiting-time jitter is $0.36\mu s$, so they are of comparable size. Since it can be shown that time jitter can be modelled as frequency modulation and vice versa, the sinusoidal jitter affecting the reconstructed service clock can be interpreted as a frequency modulation with $\Delta f = F 2\pi f_j A_j = 86\,\text{Hz}$ and $\beta = 0.02$. From this value of $\beta$ only one prominent peak in the FM spectrum would be expected: at the 'carrier' frequency ($F$) since $J_0(\beta) \approx 1$, but $J_1(\beta) \approx 0.011, J_2(\beta) \approx 5.8 \times 10^{-5}$. However, the carrier frequency peak will occur at the normalised frequency $\bar{f} = 0$ and the other peaks will fold over into the range between $\bar{f} = 0$ (i.e., effectively at the carrier frequency $F$) and $\bar{f} = 1$ since the 'FM signal' is effectively being bandpass sampled at $F$ Hz by the regenerated service clock. The peaks corresponding to $F \pm f_j$ and $F \pm 2f_j$ will occur at approximately $\bar{f} = 0.269, 0.731$ and $\bar{f} = 0.4625, 0.5375$. At the scales used to view the plots, the second set of peaks is clearly visible, and each has an amplitude of approximately $3 \times 10^{-6}$. The other peaks at $\bar{f} = 0.269, 0.731$ are located at the same point in the spectrum as the main feed-through sinusoidal jitter peaks and so cannot be easily distinguished from these. However, subtraction of the magnitudes of the simulation spectrum (which does not have these peaks) from the corresponding magnitudes of the experimental spectrum suggests that their amplitude is approximately $5 \times 10^{-6}$, which is surprising as they should be larger than the peaks at $F \pm 2f_j$. However, the discrepancy could be due to some of their amplitude being incorporated into the spectral bin corresponding to the feed-through sinusoidal jitter peak. The peak at $\bar{f} = 0$ is much larger in the experimental spectrum than in the simulation spectrum which confirms the contribution of the FM spectrum in the experimental case. For example at $\rho = 0.05$, the peak at $\bar{f} = 0$ is 0.9652, whereas the peak at $\bar{f} = 0$ in the simulation spectrum is $9.75 \times 10^{-5}$.

# IV Conclusions

The results and spectral plots presented in this paper suggest that the spectra predicted in [13] for the cases of jitter on the source and destination reference clocks in timing transfer are correct. However, experimental results also show the existence of some spectral components that were not predicted in the initial modelling as they were overlooked. The value of experimental work in validating theoretical models and assumptions in modelling is clear.

The following points are also noteworthy. In the case of jitter on the reference clock at the destination, the effect is extremely small. For high-speed clocks, even large jitter amplitudes such as 18 UI result in only small amounts of jitter on the lower rate reconstructed timing signal, for example peak-to-peak amplitude is about 0.5μs in 67.5μs or 0.7%. In the spectral domain, this translates into extremely small spectral peaks: the feed-through sinusoidal jitter peaks are only about $1.7\times10^{-3}$, the feed-through waiting-time jitter lines are of the order of $10^{-6}$ and the aliased waiting-time jitter due to the non-uniform sampling is two orders of magnitude smaller still. When jitter is present on the source destination clock, the effect is larger. The waiting-time jitter spectral peaks in the plots in Fig. 5 and Fig. 6 are of the same order of magnitude as those in Figs. 7-9, but the amplitude of the jitter on the source reference clock used to produce them was of much smaller amplitude - only 0.09 UI. The spectral pattern produced by jitter on the source reference clock is also the same as that produced by jitter on the service clock. The effect of jitter on the destination reference clock is very small because it is, understood intuitively, a second-order effect: the jitter on the destination reference clock is sampled by the reconstructed service clock. The amplitude of the jitter is also small because the unit interval is small, so the jitter is a very low-level high-frequency jitter in the distribution of the reconstructed service clock. In contrast, the effect of the jitter on the source reference clock has been shown to be entirely analogous to that of

jitter on the service clock. Although its overall amplitude may be small, also because the unit interval in question is small (i.e., compared with the case when the jitter actually is present on the service clock), its effect is, understood intuitively, a first-order effect. The jitter on the source reference clock has the same effect as if the service clock that is synchronized to create the SRTS is jittered and so the effect of the source reference clock jitter is increased because it is incorporated into the SRTS generation process.

# V. References


[1] J. C. Bellamy, "Digital Network Synchronization," *IEEE Commun. Mag.*, vol. 33, pp. 70-83, Apr. 1995.

[2] ITU-T Recommendation G.810, "Definitions and terminology for synchronization networks," Aug. 1996.

[3] ITU-T Recommendation G.813, "Timing characteristics of SDH equipment slave clocks (SEC)," Mar. 2003.

[4] ITU-T Recommendation G.825, "The control of jitter and wander within digital networks which are based on the synchronous digital hierarchy (SDH)," Mar. 2000.

[5] R. Subrahmanyan, "Timing recovery for IEEE 1588 applications in telecommunications," *IEEE Trans. Instrum. Meas.,* vol. 58, pp. 1858-1868, Jun. 2009.

[6] J. Eidson, J. Mackay, G. M. Garner and V. Skendzic, "Provision of precise timing via IEEE 1588 application interfaces," in *Proc. Int. IEEE Symp. On Precision Clock Synchronization (ISPCS) for Measurement, Control and Communication*, 2007, pp. 1-6.

[7] R. C. Lau and P. E. Fleischer, "Synchronous techniques for timing recovery in BISDN," in *Proc. GLOBECOM*, 1992, pp. 814-820.

[8] D. L. Duttweiler, "Waiting Time Jitter," *The Bell System Technical Journal*, vol. 51, pp. 165-207, Jan. 1972.

[9] J. Walker and A. Cantoni, "Jitter Analysis for Two Methods of Synchronization for External Timing Injection," *IEEE Trans. Commun.*, vol. 44, pp. 269-276, Feb. 1996

[10] M. J. Klein and R. Urbansky, "Network Synchronization - A Challenge for SDH/SONET?" in *SONET/SDH: A Sourcebook of Synchronous Networking*, C. A. Siller, Jr. and M. Shafi, Eds. Piscataway NJ: IEEE Press, 1996, pp. 242-250.

[11] R. Stephens, "Analyzing Jitter at High Data Rates" *IEEE Communications Magazine*, vol. 42, pp. S6-S10, Feb. 2004.

[12] J. Walker and A. Cantoni, "Modeling of Synchronization Process Jitter Spectrum," *IEEE Trans. Commun.*, vol. 47, pp. 316-324, Feb. 1999.

[13] J. Walker and A. Cantoni, "Modeling the Effect of Non-Ideal Reference Clocks on the Jitter Generated in Timing Transfer", *IEEE Trans. Commun.*, vol., 55, pp. 44-47, Jan. 2007.

[14] I. Zamek and S. Zamek, "Definitions of jitter measurement terms and relationships," . in *Proc. IEEE Int. Test Conference 2005 (ITC 2005)*, 2005, pp. 1-10.

[15] H. Uematsu and H. Ueda, "Implementation and experimental results of CLAD using SRTS method in ATM networks," in *Proc. of IEEE Global Telecommunications Conference 1994. (GLOBECOM '94),* 1994, pp.1815–1821.

[16] D. Hong; C.-K. Ong and K.-T. Cheng; **"**BER estimation for serial links based on jitter spectrum and clock recovery characteristics," in *Proc. of Int. Test Conference, 2004 (ITC 2004)*, 2004, pp. 1138-1147.

[17] F. Marvasti, "Spectrum of Nonuniform Samples," *Electronics Letters*, vol. 20, pp.

896-897, 11 Oct. 1984.

[18] A. Papoulis, "Error Analysis in Sampling Theory," *Proc. IEEE*, vol. 54, pp. 947-955, Jul. 1966.

[19] G. M. Garner. (2005, May 16) End-to-end jitter and wander requirements for ResE applications. IEEE 803.3 Residential Ethernet Study Group, Interim Meeting. [Online].Available:http://grouper.ieee.org/groups/802/3/re_study/public/200505/index.html

[20] S. S. Abeysekera, "Sigma-Delta Architectures for Pulse-Stuffing Synchronizers," *Int. J. Circuit Theory and Applications*, vol. 25, pp.457-467, 1997.

[21] R. M. Gray, "Quantization Noise Spectra," *IEEE Trans. Inform. Theory*, vol 36, pp. 1230-1244, Nov. 1990.

[22] ITU-T Recommendation I.363.1, "B-ISDN ATM Adaptation Layer specification: Type 1 AAL," Aug. 1996.

[23] A. W. M. van den Enden & N. A. M. Verhoeckx, *Discrete-Time Signal Processing: An Introduction.* Hemel Hempstead: Prentice-Hall, 1989.

## Acknowledgement

Experimental work was conducted at the Western Australian Telecommunications Research Institute, supported by Enterprise Ireland International Collaboration Grant (IC/2005/05) and the Western Australian Telecommunications Research Institute, Australian Telecommunications Cooperative Research Centre.

# Figures

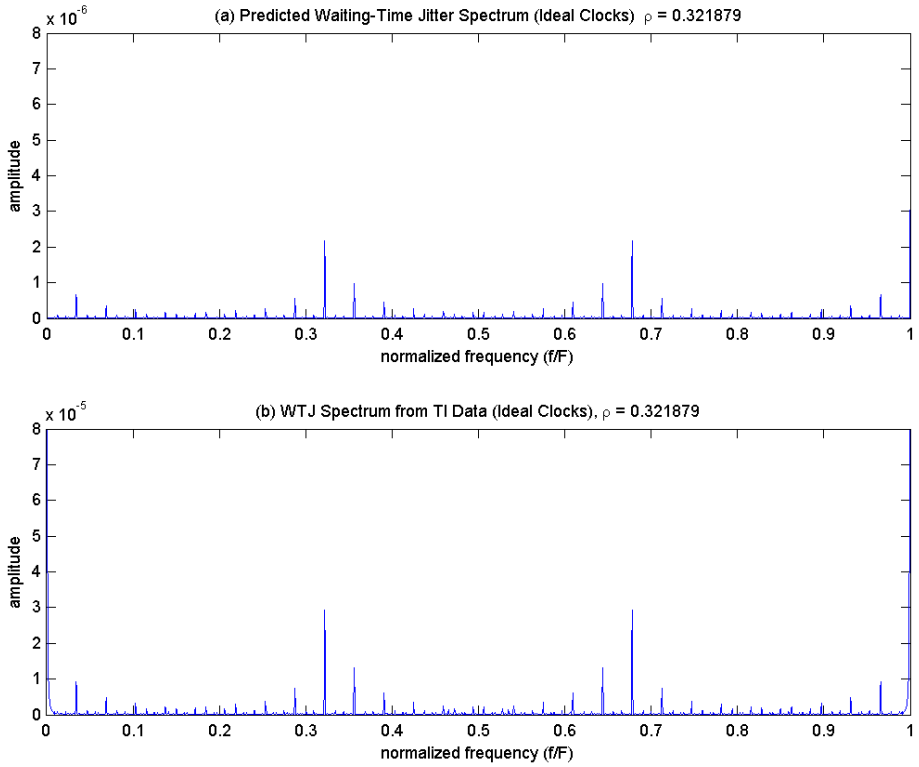


**Fig. 1: Waiting-time jitter spectrum for ideal clocks: (a) Predicted spectrum using $\rho = 0.321879$; (b) Spectrum plotted from experimental data the same $\rho$ value and unjittered clocks.**

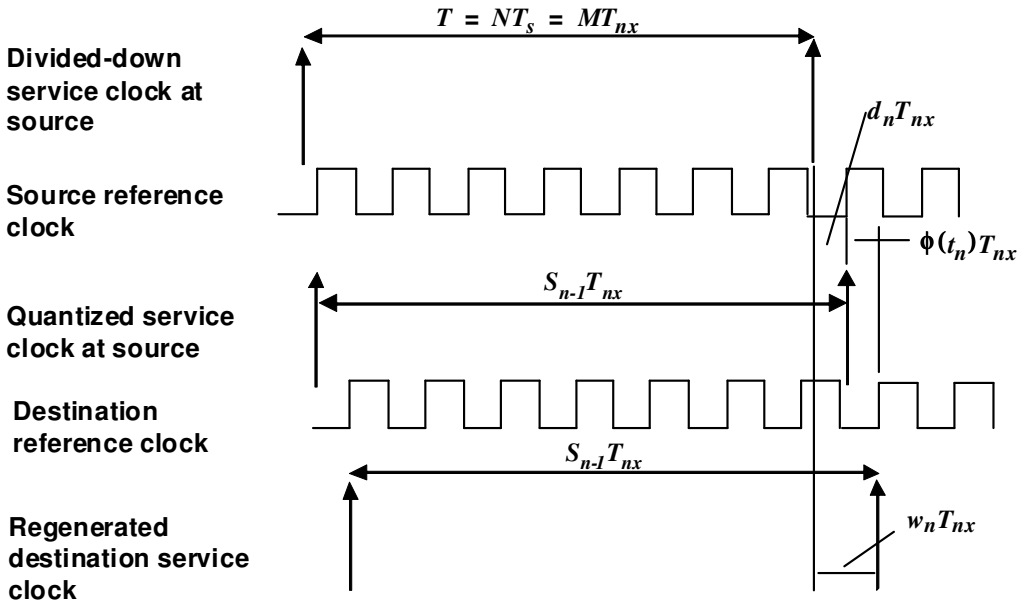


**Fig. 2: Timing diagram for synchronization process with jitter on the destination reference clock.**

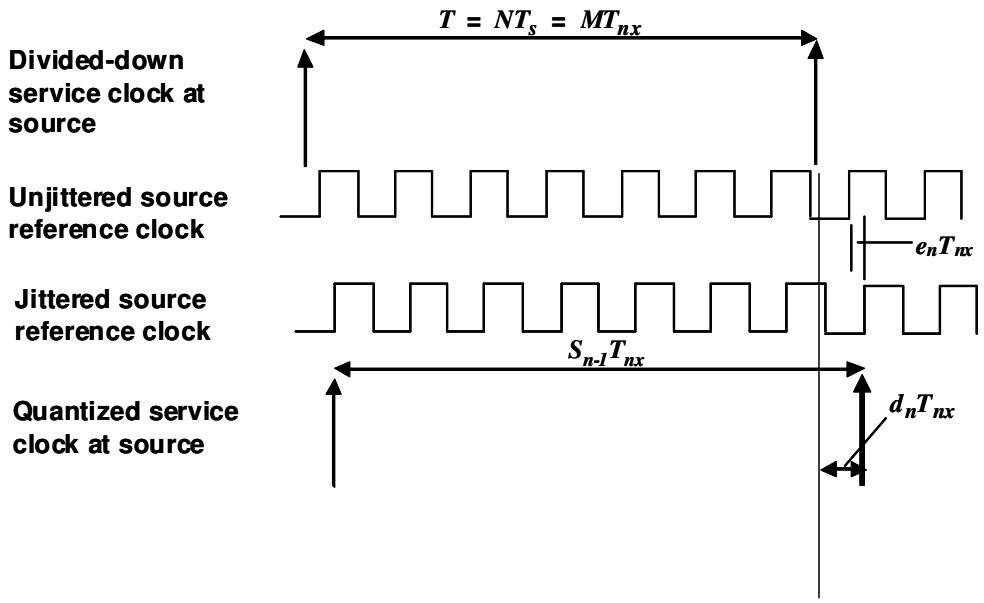


**Fig. 3: Timing diagram for jittered source reference clock showing feed-through jitter $e_n T_{nx}$.**

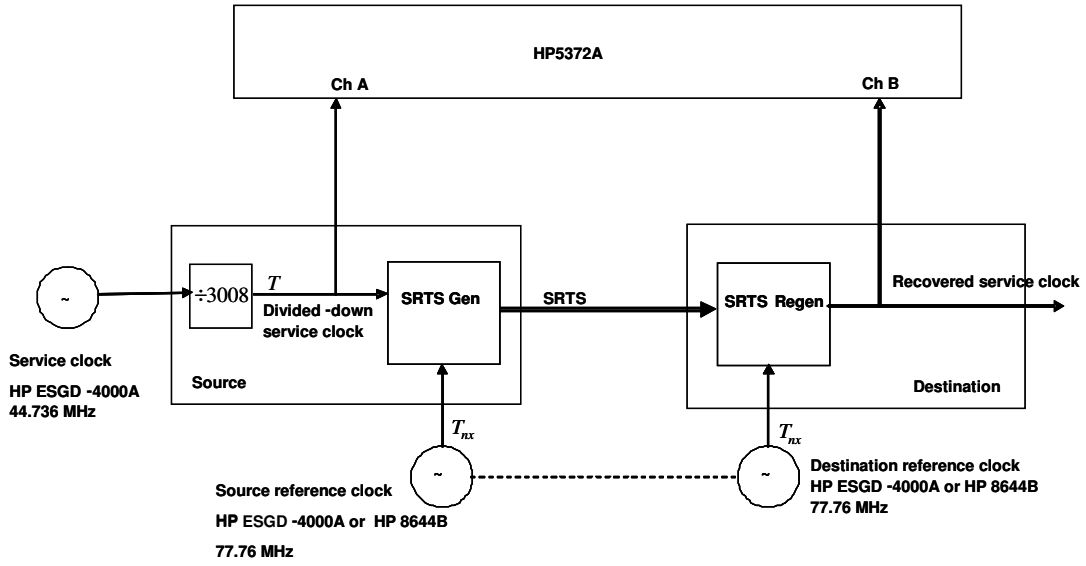


**Fig. 4: Experimental Configuration.**

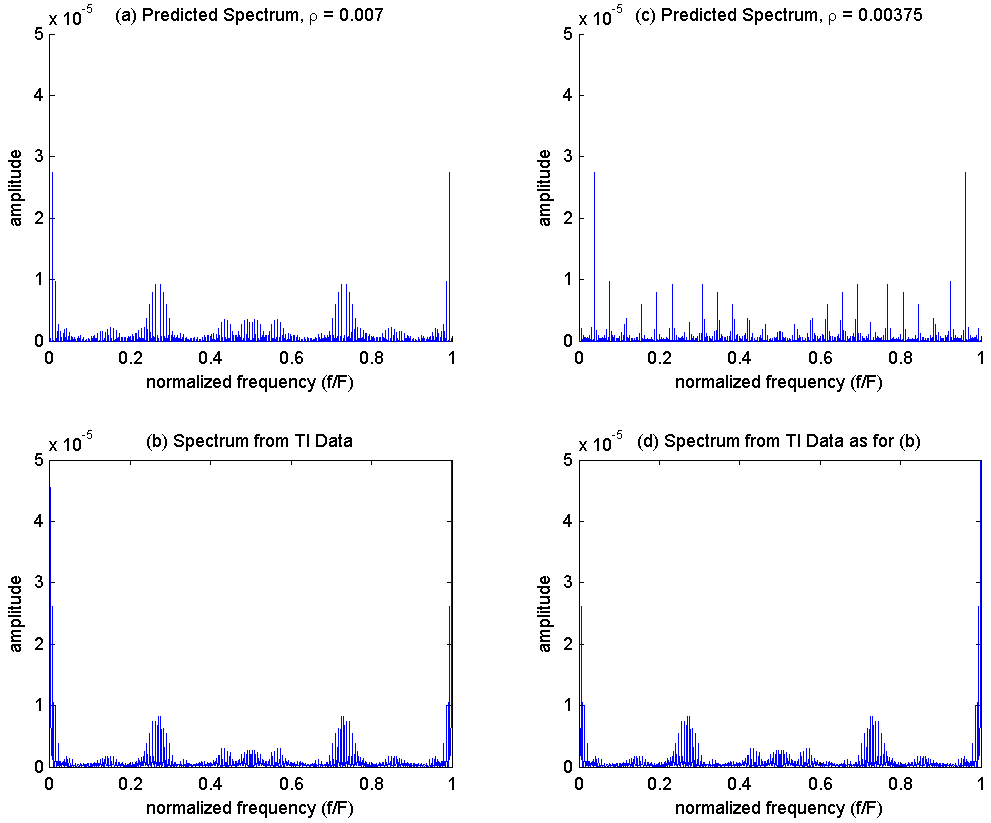


**Fig. 5: Comparison between predicted and experimental spectra: (a) Predicted spectrum using $\rho = 0.007$; (b), (d) Spectra plotted from the same experimental data with frequency settings for $\rho = 0.007$; (c) Predicted spectrum using $\rho = 0.0375$.**

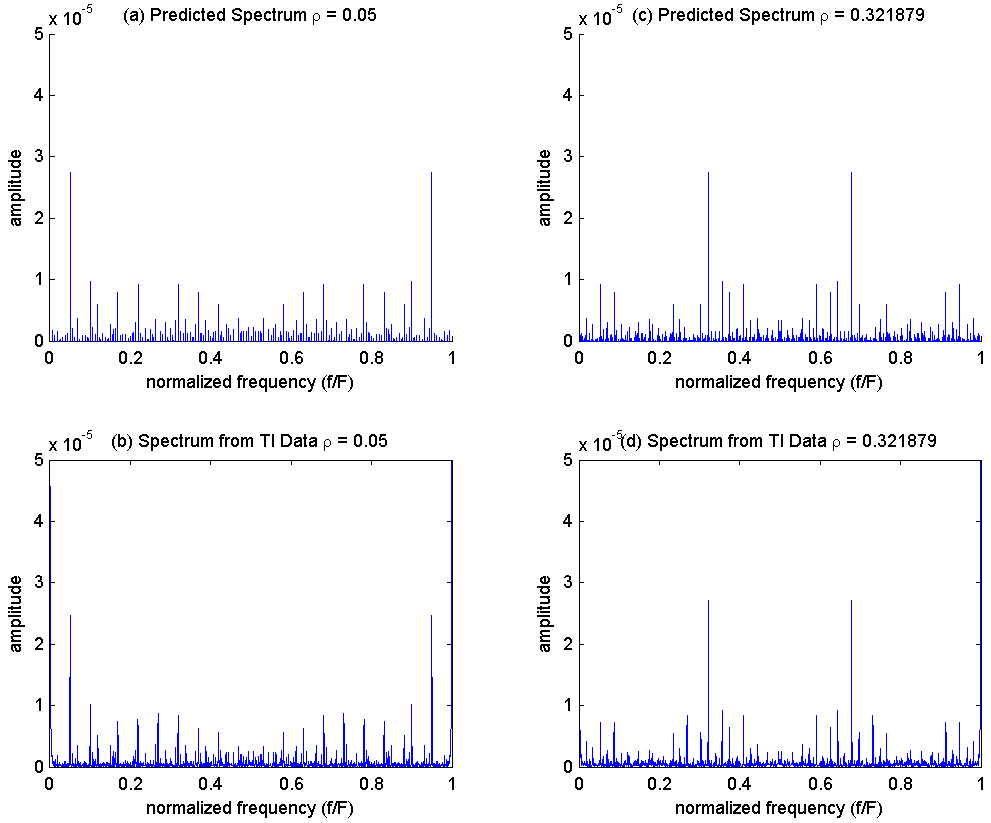


**Fig. 6: Comparison between predicted and experimental spectra: (a) Predicted spectrum using $\rho = 0.05$; (b) Spectrum plotted from experimental data with frequency settings for $\rho = 0.05$; (c) Predicted spectrum using $\rho = 0.321879$;(d) Spectrum plotted from experimental data with frequency settings for $\rho = 0.321879$**

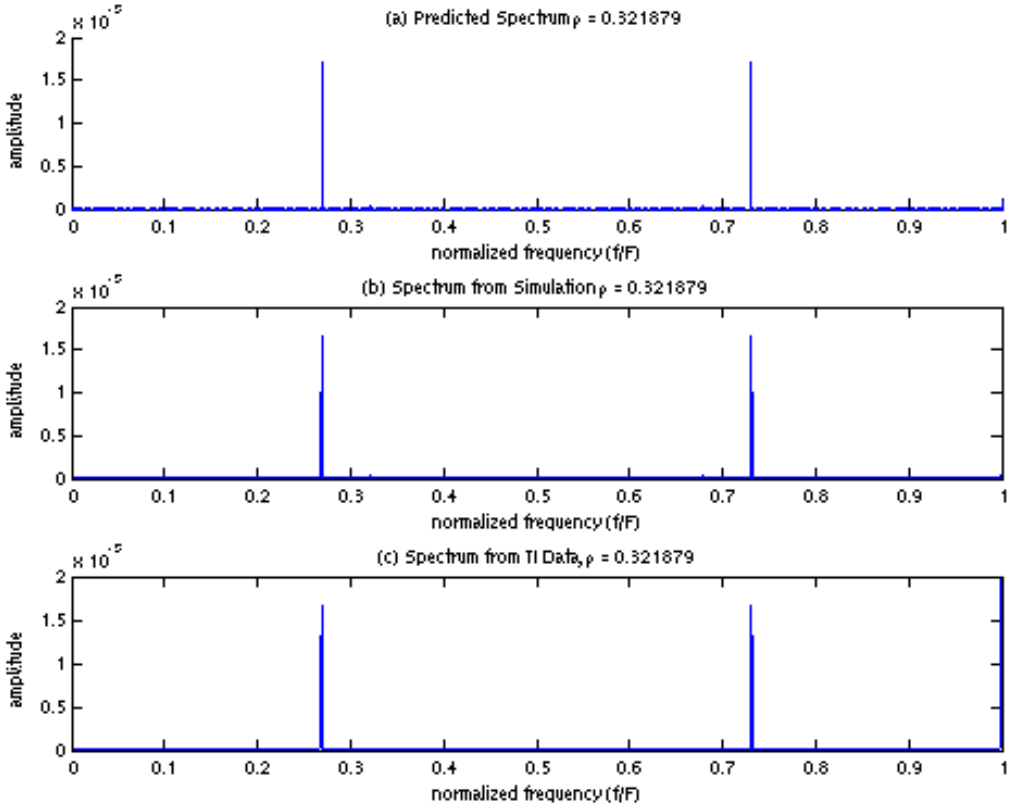


**Fig. 7: Comparison between predicted, simulated and experimental spectra: (a) Predicted spectrum using $\rho = 0.321879$; (b) Spectrum plotted from simulated data $\rho = 0.321879$; (c) Spectrum plotted from experimental data with frequency settings for $\rho = 0.321879$.**

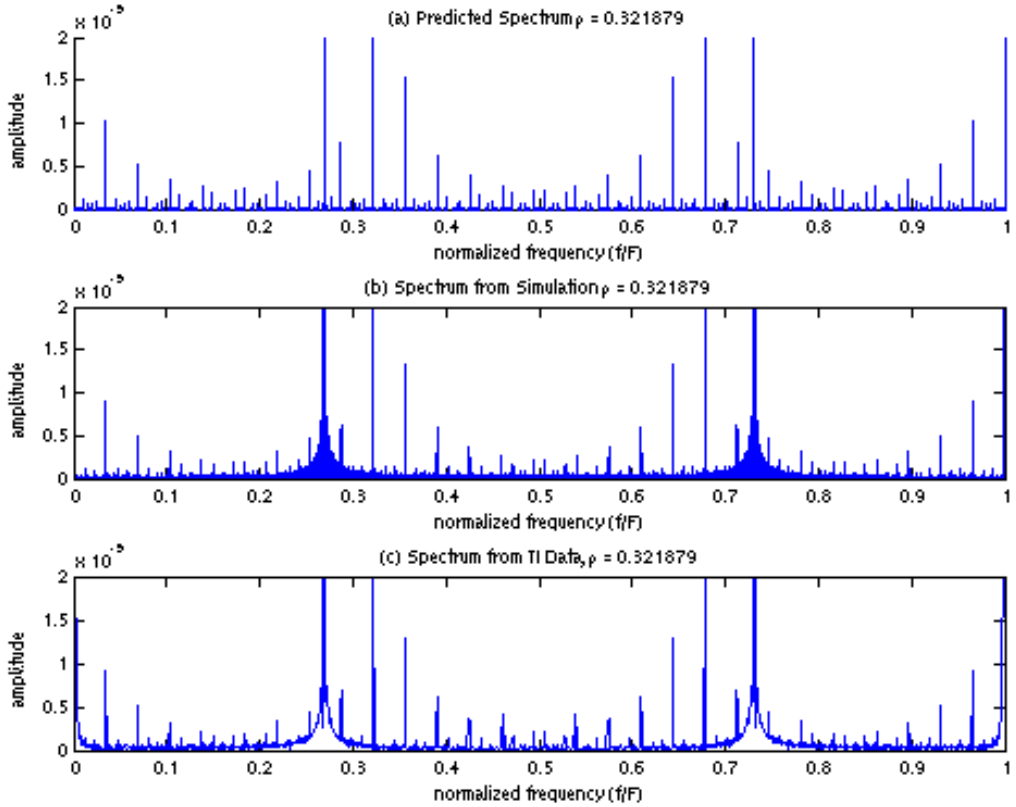


**Fig. 8: Close-up comparison view of predicted, simulated and experimental spectra. Vertical axis maximum = $2\times10^{-5}$: (a) Predicted spectrum using $\rho = 0.321879$; (b) Spectrum plotted from simulated data $\rho = 0.321879$; (c) Spectrum plotted from experimental data with frequency settings for $\rho = 0.321879$.**

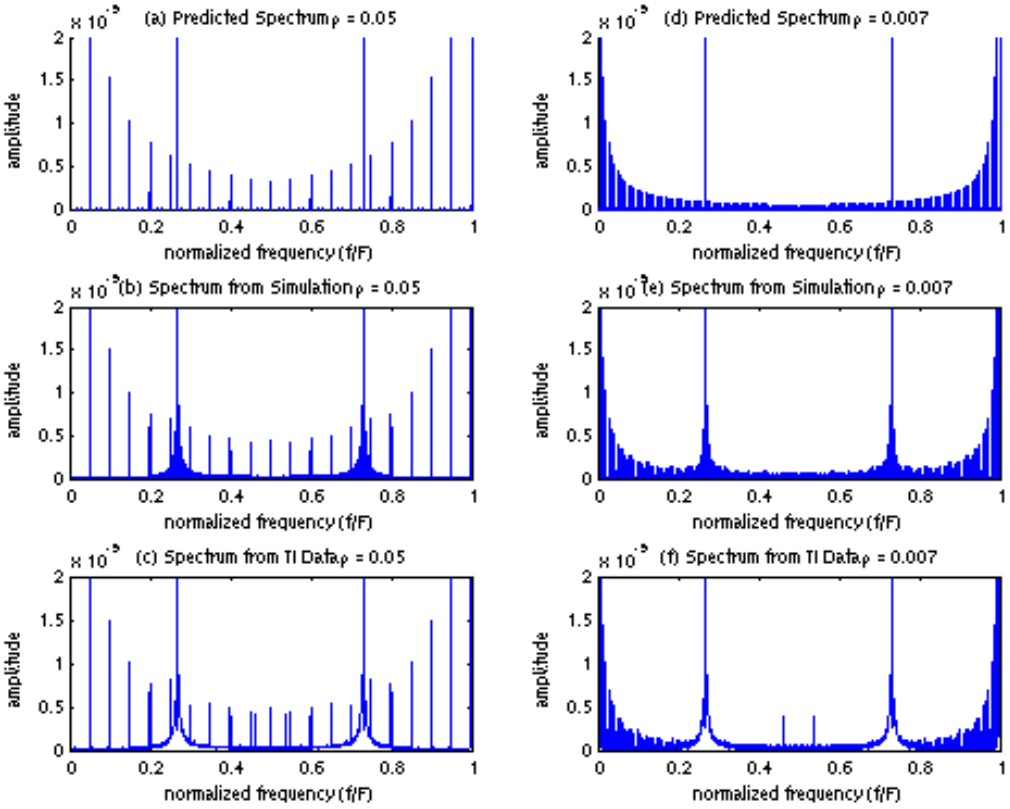


**Fig. 9: Comparison of spectra for $\rho = 0.05$ and $\rho = 0.007$: (a), (d) predicted; (b), (e) from simulation; (c), (f) from experimental data.**